Chapter 6

Modeling, Compensation and Control of Smart Devices with Hysteresis

Daniele Davino, Alessandro Giustiniani and Ciro Visone

Additional information is available at the end of the chapter

http://dx.doi.org/10.5772/51388

1. Introduction

The chapter aims to provide a review on the basic issues concerning the techniques to handle innovative devices employing materials with hysteresis and the related control strategies.

Nowadays, the great availability of materials designed to gather different physical characteristics (electric, magnetic, mechanic, etc.) working together to provide improved capabilities, has determined a huge rise of devices able to integrate different "coupled" functionalities into the same device. In this respect, the set of these "smart" or "multi-functional" materials and the devices employing them is really huge in number and quality. With no claim of exhaustivity, we can recall, for sake of example, thermo-electric, [11], or magneto-caloric [33] effects, where a coupling between Entropy/temperature and electric or magnetic fields is observed, and which promise new devices for heat recovery or refrigeration tasks, through the exploitation of new and more effective materials.

Other materials, conversely, are able to couple mechanical quantities (i.e. stress and strain) to electric or magnetic fields so amplifying the application range for actuation or sensing aims. The most known and widespread are the piezo-electric alloys ($Pb[Zr_xTi_{1-x}]O_3$, $PbTiO_3$), which show increased piezoelectric properties so allowing to make smart devices, otherwise unrealizable, [34], [32], [2]. A similar behavior is shown by the electro-active polymers, [3] which, exploiting the characteristics of polymers, allow to foresee really innovative applications. Materials with magneto-elastic coupling show a complementary behavior with respect to the former and enable to further increase the already huge set of potential smart applications. It is worth to recall the magnetostrictive materials, such as Terfenol-D or Galfenol, [21], exploited for actuation or sensing purposes, or the Ni-Mn-Ga alloys, which presents different magneto-elastic behavior and, even if less assessed than classical magnetostrictives, promise very interesting application, [37].

Omitting electro- or magneto-rheological materials and many others, we would finally mention Ni-Ti alloys showing a thermo-mechanical coupling by the exploitation of the Austenite-Martensite phase transition that enables to realize further and interesting smart devices, [31], [4]. In summary, the interest and attention of researchers and inventors is so

focused on these materials and their applications, that everyone can experience, navigating on the web, an impressive "blooming" of ideas and proposals. The key element is the consciousness that smart materials achieve new functionalities going well beyond the "sum" of the individual properties and allowing to develop new and really innovative devices.

Among them, those materials coupling mechanical to other physical quantities (thermal, electric or magnetic) received a special attention since their suitability for sensing or actuation goals. The latter involved many researchers in a multi-disciplinary frame in designing and producing really smart actuators, able to provide high forces, or high precision *micropositioning*, or high speed responses, in dependence of the selected application.

In particular, as we can find in the scientific literature, the employ of Piezo-electric materials, [23], or magnetostrictives, [21], which are able to cover complementary sets of applications, play a primary role and many devices suited for micropositioning, active vibration control, smart actuation, ultrasonic generators, are available.

Similar conclusions can be drawn for Shape Memory Alloys (SMA) which show huge deformations driven by temperature variations and therefore are generally quite slow [45]. The Ni-Mn-Ga materials, also referred to as Ferromagnetic Shape Memory Alloys (FSMA), [40] overcome this limitation still preserving high deformations as SMAs.

However, all of them, share *rate independent* memory properties which strongly affect the global behavior of the device and its performances. Rate independence means that the observed memory behavior doesn't arise from "dynamics" and therefore is still kept also for "quasi-static" input variations, as happens in the well-known behavior of ferromagnetic materials. The common way to refer to it is *hysteresis*.

In the sequel, a strategy to "handle" devices employing smart materials with hysteresis in general working conditions will be outlined and several applications employing magnetostrictives will be discussed to check the validity of the proposed techniques.

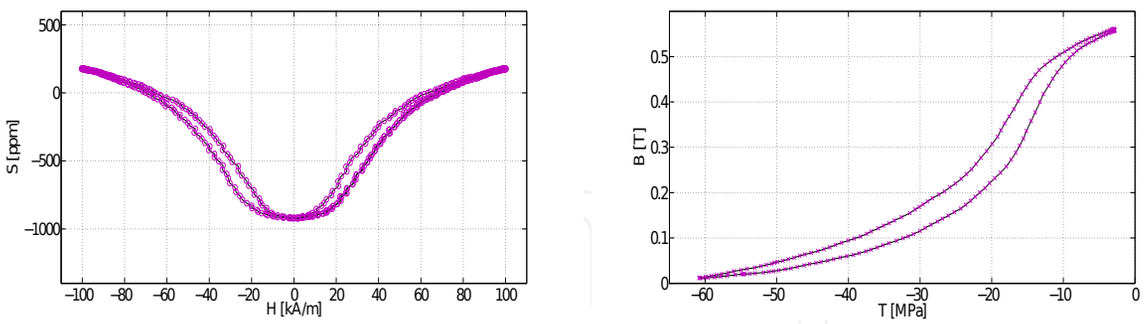

(a) Magnetostriction at constant stress (b) Inverse Magnetostriction at constant field

Figure 1. Elastic and magnetic response of a Terfenol-D sample to a magnetic (a) or mechanical (b) input

2. Hysteresis operators and their basic properties

The general approach to materials showing nonlinear coupling and hysteresis between the involved variables, can be written as

$$y_1 = \mathcal{F}_1(x_1, x_2), \tag{1}$$

$$y_2 = \mathcal{F}_2(x_1, x_2), \tag{2}$$

being (x_1, x_2) the couple of input variables, and (y_1, y_2) the couple of output variables. Of course, the choice of input and output variables is, in principle, arbitrary and is performed according to the specific application needs. Moreover, $\mathcal{F}_1$ and $\mathcal{F}_2$ represents arbitrary and general operators with memory, which "link" the input to the output functions. This is a quite generic picture, by which we would just acquaint the reader on the complex phenomena lying below the behavior of such materials. In particular, we would evidence that, generally speaking, equations above define a *multi-variate operator* with memory which could be handled by means of *vector operators* with hysteresis, [28], [25]. Unfortunately, they require huge efforts in identification procedures and high computational weight, so resulting unsuitable for *sensing* or *actuation* tasks. As a consequence, other approaches have been considered with the aim to gather good generality and modeling capabilities to a relative simple handling and computational effort, [28], [1], [42]. There, the basic concern was to fully exploit the "machinery" of the classical hysteresis operators, well suited to link together *one input* to *one output*. They are usually referred to as SISO (Single Input-Single Output) systems. As a starting point, any functional material can be modeled as a SISO system whenever only one of the output variables is of concern and, moreover, one of the inputs is kept constant. For the sake of example, Fig.1-(a) and -(b) sketches the typical elastic response driven by magnetic field or the flux density induced by applied stress, respectively. In each of these pictures, a specific characteristic with memory is described and can easily be modeled through a classical SISO hysteresis operator. In a more general framework, as shown in Fig.2-(a) and -(b), a SISO modeling is still applicable whenever the interest is only on one of the output variables (i.e. the *strain* in picture -(a)), and when *stress* can be assumed as stationary (same picture). Of course, the same reasoning can be applied when the *flux density* as output variable is of concern (picture -(b)). A quite unifying approach to define a wide class of hysteresis operator

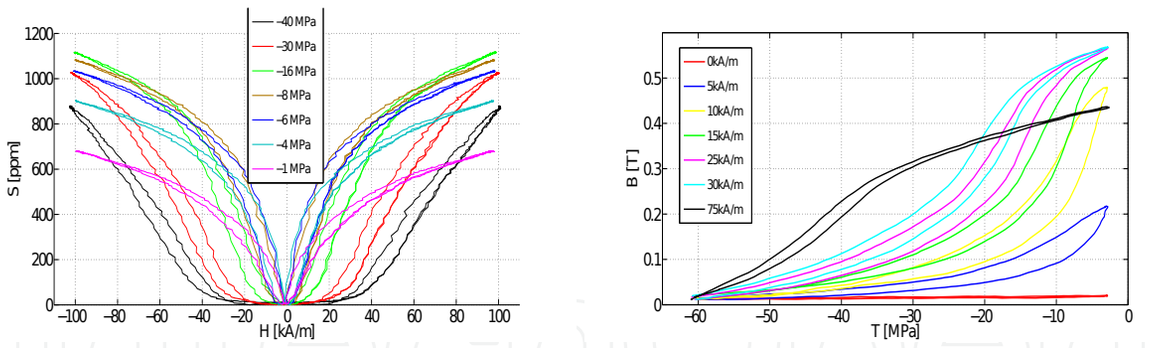

(a) Magnetostriction as function of stress

(b) Inverse Magnetostriction as a function of magnetic field

Figure 2. Elastic and magnetic response of a Terfenol-D sample to a magnetic (a) or mechanical (b) input at various magnetic fields and stresses

is based on the *Preisach memory* updating rules, [28], [25] and we refer to them in the sequel. For the sake of simplicity and assuming some basic knowledge on the Preisach operator, we can introduce the Preisach hysteresis operator as the superposition of a continuous set of ideal relay operators, $\hat{\gamma}_{rs}$ defined by the parameters $r \in \mathbb{R}^+$ and $s \in \mathbb{R}$ as specified in the Fig. 3. Here it should be noticed that the *relay* can be represented by means of the r and s parameters, or by its switching fields a and b ($a \geq b$), equivalently. In the latter case the formalism is the one exploited by I.D. Mayergoyz in [28], while the former yields to the formalism used in the books [7, 26] and one can be derived from the other by a simple 45° axis rotation, [44]. In the

sequel we decided to use the second approach which allows the reader to refer to those books so exploiting several results there addressed. On the contrary, this choice has the drawback to discuss some tool of the Preisach formalism (i.e. identification, or inversion algorithms) in a less natural way. For this reason we would further evidence the aim of this chapter, focused in providing a sufficiently complete discussion concerning the modeling and compensation of systems with hysteresis and referring for details to the cited references.

Each *relay*, referred to $R_{r,s}[x]$, has $r \geq 0$ and $s \in \mathbb{R}$. We assume now that they are distributed into the $\mathbb{R}^+ \times \mathbb{R}$ half plane with a prescribed distribution function $\mu(r,s)$ and the output of this set is the linear weighted superposition of the response of each *relay*. In symbols, [28], [25], [26]:

$$y(t) = \iint_{\mathbb{R}^+} \mu(r,s) R_{r\,s}[x](t) dr ds \tag{3}$$

Of course the past input history of each relay of the distribution results in a non trivial way to compute the integral. However, this problem can be overcome by giving a geometric interpretation to it. First of all, let us associate to each point of the half plane (r,s) the relay having the same parameters. Moreover, recall that each relay of the distribution switches from the state -1 to $+1$ if the input field exceeds the upper switching point, that is $x(t) \geq s + r$, while the opposite transition from positive to negative output is performed if the field is below the lower switching point or, in symbols: $x(t) \leq s - r$. This yields to the following conclusion: the relay operators switched to the $+1$ state are those below the straight line of equation $s + r = x$; conversely, those switched from the state $+1$ to -1 lie above the line $s - r = x$. If all the relays start from the state -1 (usually referred as the state of *negative saturation*) and applying the input field $x(t)$, the line separating the $+1$ from the -1 elements is sketched in Fig. 3-(b) and represents the state of the system. When, from such initial state,

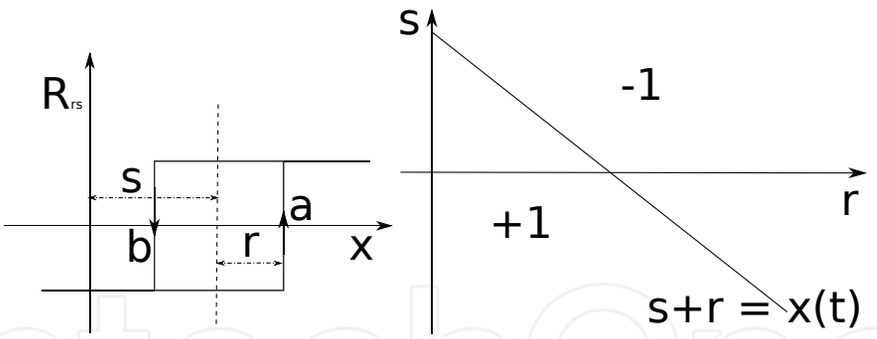

Figure 3. (a) The ideal relay with parameters r and s; (b) geometrical interpretation of the relay switching

the input is decreased, the relays above the line $s - r = x(t)$ switch down to -1. The result is sketched Fig. 4-(a), while in Fig. 4-(b) it is represented the state corresponding to an arbitrary *non-monotone* input variation. The *demagnetized* or *virgin state* is represented in the $\mathbb{R}^+ \times \mathbb{R}$ half plane as the horizontal axis ($s = 0$). We will refer to it as the h_0 state.

After this brief resume, it should be quite easy to realize that the above mentioned rules define a specific relation between the set of continuous input functions, $x(t)$ and the piece-wise linear function $h(r,t)$, as follows:

$$\Theta : x \in \mathcal{C}^0[0,T] \rightarrow h(r,t) \in \Psi_0, \tag{4}$$

with, h the staircase of the classical Preisach model (cfr.[28]), and Ψ_0 the set of admissible Preisach states. The properties of this operator, referred to as Preisach Hysteresis Generator (PHG), can be easily sketched. To this aim, let us consider the functions $x(t)$ and $z(t)$, shown in Fig. 5-(a), sharing the same sequence of input extrema and linked by the equation $x(t) = z \circ \rho(t)$. The function ρ is a time rescaling and $\circ$ the composition operator. In other words the two functions differ only by the rate of variation. It is easy to verify that the staircases corresponding to x and z coincide (Fig. 5-(b)). The memory operator, therefore, is not affected by the input rate, but only by the sequence of the input extrema.

Let us now consider the memory operator with initial state equal to the h_{-1} *virgin state*, i.e. $h_0 = h_{-1}$ undergoing the input $x(t)$, shown in Fig. 5-(a). The vertex of the staircase (x_3, x_4) are wiped out as soon as the input exceeds x_3 as they were never existed, as shown in Fig. 5-(b). The final state generated by the sequence of input extrema $(x_1, x_2, x_3, x_4, x_5)$ coincides with the one generated by the *reduced* input sequence (x_1, x_2, x_5), [41]. The latter is the basic rule for memory updating which is universally referred to as *Preisach deletion rule*. In conclusion, the Preisach-memory operator is *rate independent* and fulfills the *wiping-out* property. What we have just introduced is the machinery enabling the classical Preisach operator, defined in eqn. (3), to take into account *rate-independent* memory phenomena. To

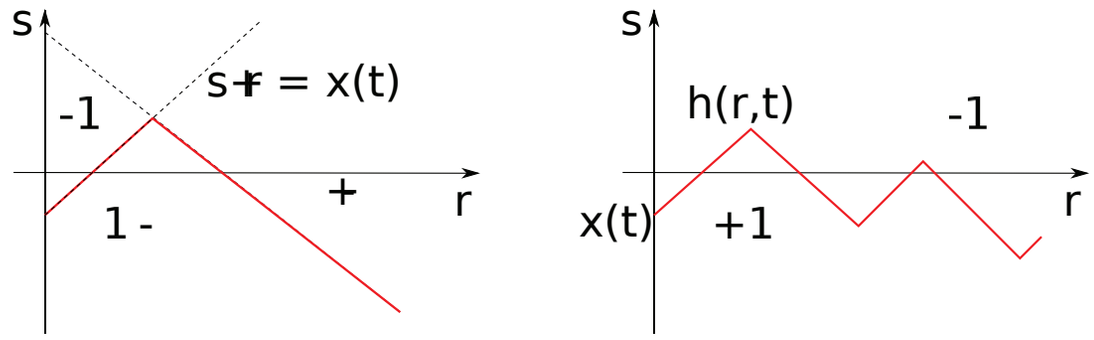

(a) (b)

Figure 4. (a) staircase in the case of non-monotone input variation (b) Staircase corresponding to a non-monotone input $x(t)$

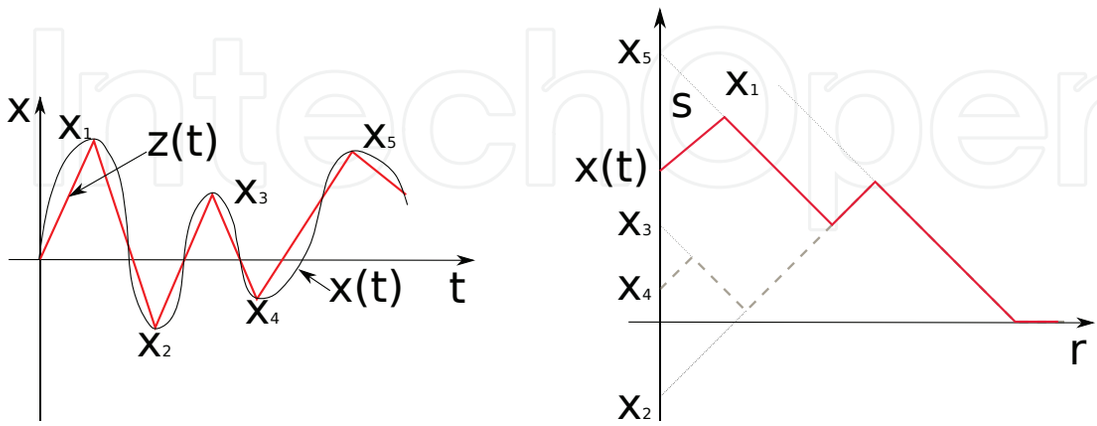

(a) (b)

Figure 5. (a) staircase in the case of non-monotone input variation (b) Staircase corresponding to a non-monotone input $x(t)$

fully exploit such operator, it is possible to define a larger class of operators with hysteresis, based on the Preisach memory updating rules, as proposed in [7], where any operator with Preisach memory can be represented as follows:

$$\mathcal{W} = F \circ \Theta, \tag{5}$$

where Θ is the PHG, while

$$F : h(r,x) \in \Psi_0 \rightarrow y(t) \in \mathbb{R}. \tag{6}$$

represents a memoryless functional by which a wide class of hysteresis operators, based on the Preisach memory, can be defined. It should be noted that this formalism, adopted in [7, 26], is slightly different with respect to [28], representing the Preisach plane by means of a rotated coordinate system, [44]. For the sake of example, the following functional

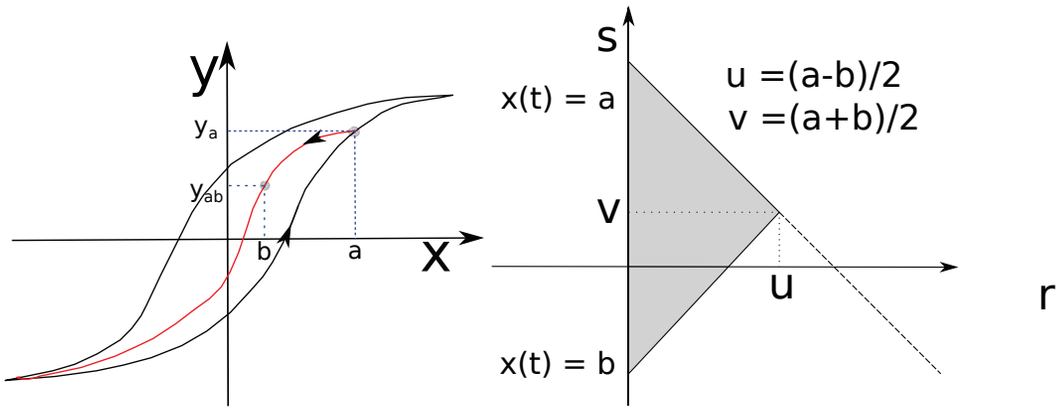

(a) Definition of first order reversal curve (b) Triangular domain over which the Everett integral is defined

Figure 6. Identification procedure of a Preisach model, based on the exploitation of first order reversal curves

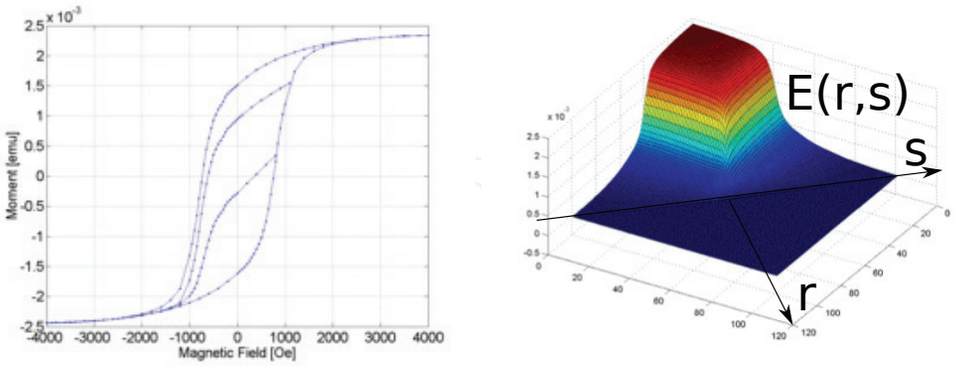

(a) Characteristic of a floppy disk (b) Everett function of a floppy disk

Figure 7. Example of the identification of the Everett function from experimental data coming from a floppy disk

$$F : h \in \Psi_0 \rightarrow \int_0^{+\infty} dr \left(\int_{-\infty}^{h} \mu(r,s)ds - \int_h^{+\infty} \mu(r,s)ds \right), \tag{7}$$

defines the Classical Preisach operator, and $\hat{\mu}(r,s)$ is a density function to be determined. The functional

$$F : h \in \Psi_0 \rightarrow \int_0^{+\infty} \mu(r,s)h(r,t)dr, \tag{8}$$

conversely, defines the well known Prandtl-Ishilinskii operator [7]. Such models have been widely exploited in last years by several authors to compensate the memory of real devices, so allowing a model-based control approach. A non exhaustive review can be found in [44]. It should be quite evident that these models are phenomenological in nature and so require well-defined identification procedures to link their parameters (i.e. the mapping functional, F) to the real material, through a suitable set of measured data. It should be said that such a procedure is not addressed for any arbitrary functional, while, in the case of the Preisach operator, a simple and well-behaved identification procedure is available and, for convenience it is reported with some detail hereafter.

In particular, it could be observed that in order to compute the output of a classical Preisach model, it is not necessary to know the Preisach Distribution Function, $\mu(r,s)$ [28], but it is sufficient the knowledge of the integrals of $\mu(r,s)$ over any triangle of the $\mathbb{R}^+ \times \mathbb{R}$ half plane and vertex (u,v), according to the procedure described below. Preliminary, let us define the following function known as *Everett function*, as follows:

$$\mathcal{E}(u,v) = \int_0^u dr \left(\int_{v-u+r}^{v} \mu(r,s)ds + \int_v^{v+u-r} \mu(r,s)ds \right). \tag{9}$$

The link between the actual measured data and the Everett function can be outlined as follows. Let us start from negative saturation and increase the input until the value $x(t) = a$ and the corresponding output is y_a are attained. Then decrease the input until the value $x(t) = b$ is reached; the corresponding output is referred to as y_{ab}. The hysteresis branch (Fig. 6-(a)) traced from the reversal point y_a until, again, the negative saturation is known as *first order reversal curve*, or *for*-curve. It is easy to realize (cfr. also [28]) that the following relation linking the output measured data and the Everett integral holds:

$$\mathcal{E}(u,v) = \frac{y_a - y_{ab}}{2} \tag{10}$$

with

$$u = \frac{a-b}{2} \tag{11}$$

$$v = \frac{a+b}{2}. \tag{12}$$

Let us subdivide the input interval into N equal intervals of width $\Delta x = x_{max} - x_{min}$ and assume $x_1 = x_{max} = N\Delta x$, $x_k = (N-k+1)\Delta x$. The corresponding reversal curve (Fig. 6-(b)) so has $N-k+1$ measured points, $y_{a_k b_n}$. Hence the total number of measured points to be used for the identification procedure, are $N \times (N-1)/2$, which correspond to the number of nodes in the grid in the $\mathbb{R}^+ \times \mathbb{R}$ half plane. Now, if we associate the value of the Everett integral to each point of the grid, a discrete version of the Everett function is easily available. The details on its construction and use can be found in [28]. An example of the reversal curves for a real material, and the corresponding Everett function is shown in Fig. 7.

3. Compensation algorithms

The definition of suitable control algorithms to be embedded in actuators employing smart materials is sensibly affected by the memory phenomena involved. This because, roughly speaking, the controller has no memory of past history which, conversely, affects the plant behavior, and will be not able to provide suitable correction to track a desired trajectory. The system therefore will show poor performances. A simple way to overcome this problems, proposing quite a simple control strategy, is based on the following well known issues. As a preliminary step, let us assume that the plant is adequately modeled by the series connection of a hysteresis operator and a linear dynamic component. In Fig. 8-(a) it is shown a control scheme employing a generic nonlinear controller which gather both dynamics and *rate-independent* properties, even if specifying its details is non-trivial. Let us assume that the *rate independent* behavior of the plant can be modeled by the aid of a hysteresis operator $W[x]$, as defined in section 2. If the inverse of the hysteresis operator partly modeling the plant were available, their series connection in the control scheme bears to a linear system, allowing the employment of all standard linear control strategies, as shown in Fig. 8-(b). In summary, in order to simplify the controller design, it is suitable to compensate nonlinearity and *rate-independent* memory of the actuator. This approach is generally referred to as *model-based* control strategy. The issue is now to address the definition of the compensator of a hysteresis

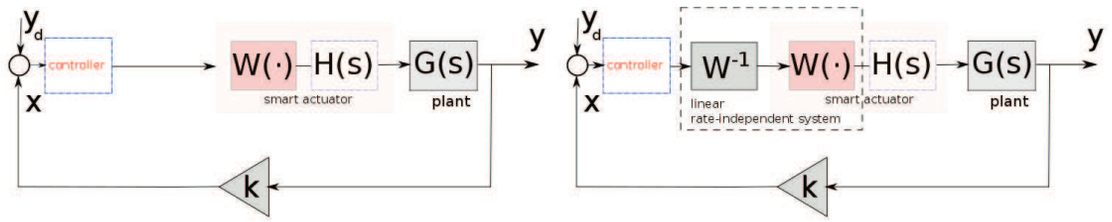

(a) The general controller should take into account memory effects

(b) Model-based control scheme: a suitable modeling of the plant is performed which enable to provide a compensator

Figure 8. General control scheme (a) - Model-based control scheme (b)

operator and to define the conditions under which such an operator admits an inverse or *compensator*,[7, 27]. In particular:

Definition 1. *A hysteresis operator $\mathcal{W}^{-1}$ with initial state $\phi_{-1} \in \Psi_0$, is called a* compensator *(or inverse) of the operator $\mathcal{W}$, with initial state ψ_{-1} if, for any state $\phi \in \Psi_0$, there is a state $\psi \in \Psi_0$, such that $\mathcal{W}_\psi \circ \mathcal{W}_\phi^{-1}\, x(t) = \mathcal{W}_\phi^{-1} \circ \mathcal{W}_\psi\, x(t) = x(t)$, for every input function x(t).*

Of course, the above definition lead us asking the conditions making this issue sound. This requires to specify the hysteresis operator with more detail. To this aim, we refer to the class of operators based on the Preisach deletion rule, stated in eqn. (5). We refer to this operators, to as $\mathcal{P}_0$-operators. In particular, we can define a piece-wise strictly monotone operator of this class, [7], according to the following

Definition 2. *The operator $\mathcal{W} = F \circ \Theta$ with initial state ψ_{-1} mapping the set of continous functions, $\mathcal{C}[0, T]$, into itself, is piece–wise strictly increasing if*

$$[F(\Theta(x, \psi) - F(\psi)]\,[x - \psi(0)] > 0, \quad x \neq \psi(0), \tag{13}$$

where $\psi(0)$ is the past input, while the symbol $\Theta(x,\psi)$ is the staircase attained by starting from ψ and applying the value of input x at time t.

Such a property guarantees the invertibility of $\mathcal{P}_0$-operators and is connected to the specific memoryless mapping functional F. It turns to the classical definition of monotonicity for the (single valued) hysteresis branch when the state (i.e. the staircase in the Preisach plane) is specified. In the particular case of the classical Preisach operator, with mapping functional specified in eqn. (7), the following theorem holds [6]:

Theorem 1. *The Preisach operator, $\mathcal{H} \in \mathcal{P}_0$, in eqn. 3 with distribution function μ, admits an inverse if and only if $\mu \geq 0$, and $E(u,v) \geq 0$, for every $(u,v) \in \mathbb{R}^+ \times \mathbb{R}$.*

Before discussing an efficient algorithm to implement the inverse of Preisach operator, it is important asking why the inverse operator cannot be employed by just exchanging the role of input and output.[1] In principle, this is not accurate, due to a specific property of the Preisach mapping functional, known as *congruency*. Let us refer to Fig. 9-(a), where it is sketched the state updating corresponding to the same *up and forth* input variation (from x_- to x_+) for two different states h_1 and h_2. It is quite evident that two minor loops are generated, each corresponding to an initial state, and they are *congruent* by vertical translation, Fig. 9-(b). The inverse operator describe a characteristic which is placed symmetrically to the direct characteristic, with respect to the $y = x$ line. As a consequence, any minor loop described by the model is transformed into one which is symmetrically placed with respect the same line.This implies that two congruent minor loops generated by the model, are transformed by the inverse operator into two minor loops which are congruent by a horizontal translation. Fig. 10-(a) illustrates such a situation. Conversely the operator which just exchanges the

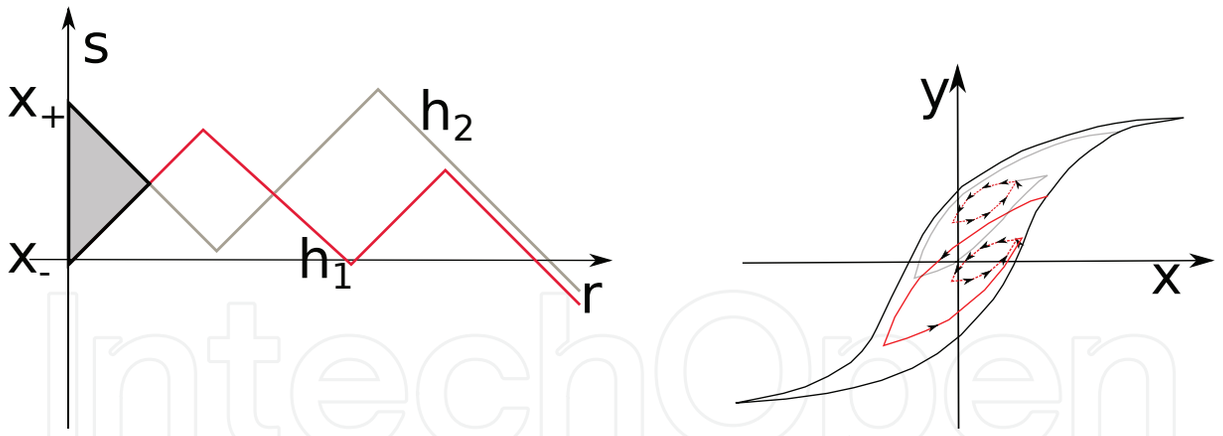

(a) States corresponding to the same up and forth input variation (b) Congruent minor loops

Figure 9. Illustration of the Congruency property of the Classical Preisach Problem

role of the variables that we call *pseudo-compensator* is still a Preisach operator and therefore generates vertically congruent minor loops, as shown in Fig. 10(b). It is so manifest that this operator cannot be strictly considered as the inverse of a Preisach operator, due to the limitations imposed by the congruency property. However this observation doesn't limit the possibility to adopt pseudo-compensator as a hysteresis model by itself which is able to

[1] In reality this is a procedure to define and approximation of the inverse, referred to as *pseudo-compensator* as detailed in [30]

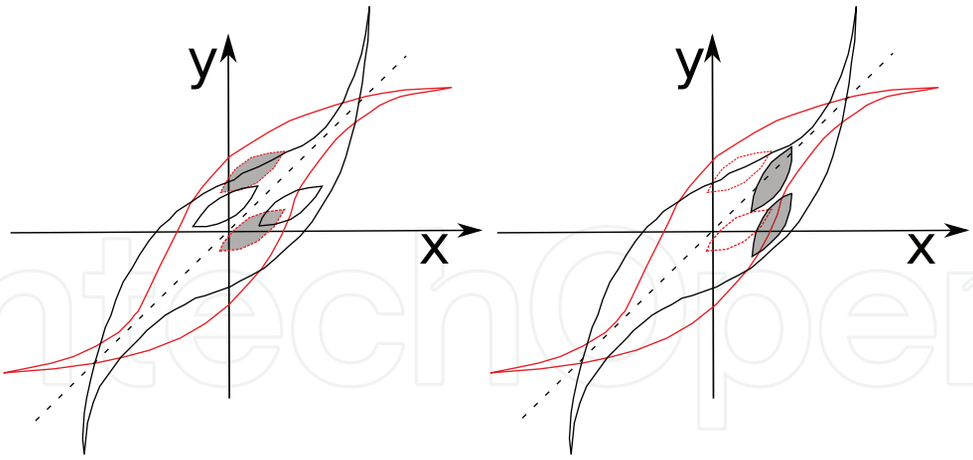

(a) States corresponding to the same up and forth input variation

(b) Congruent minor loops

Figure 10. Illustration of the Congruency property of the Classical Preisach Problem

guarantee good performances, as widely described in [20, 29]. In summary, the *inverse* of a classical Preisach operator *is not* a Preisach operator; the pseudo-compensator, conversely, *is* a Preisach operator and cannot rigorously represent the Preisach compensator.

It should be stressed that even if the inverse of the Preisach operator exists, it is not possible, generally speaking, to represent the compensator in a closed form, except than in very specific cases, [44], [26], [27], [43]. So it is mandatory the definition of well-defined and computationally efficient inversion algorithms in general working conditions. To this aim we will briefly sketch the issue, by referring to [12, 44] for details. When the conditions of invertibility of the Preisach operator are fulfilled the problem of finding its inverse has sense and the inversion procedure is based on the algorithm of state updating which assumed the output $y(t)$ as known. In other words, the algorithm described hereafter, allows to provide the input field of the operator at time instant t, corresponding to a given and known output $y(t)$, once the initial state is assigned. This procedure, since no numerical iterations are needed, allows to compute the inverse with the same computational efficiency and accuracy of the classical algorithm used to compute the Preisach operator. For this reason we refer to it as a "fast" inversion algorithm, [13] [14]. If the Preisach plane is divided into a $\Delta x \times \Delta x$ mesh, with $\Delta x = \frac{x_{max} - x_{min}}{N}$ then the Everett function is uniformly sampled into a $(N+1) \times N/2$ mesh, as sketched in the Fig. 11. Therefore the solution of the above equation can be performed by a simple inspection of a look-up table, according to the rules described below. Moreover, let us assume that the Everett integral is limited to the triangle ABC. This is a quite reasonable hypothesis, since the function must vanish at infinity. In the same plane, it can be evidenced the initial state of the operator, $h_0(r,t)$. Let us further assume the output $y(t) = y_0 + \Delta y$, is known. In the ordinary fashion of handling the Preisach operator, the output variation Δy coincides with the integral of the distribution function over the area S, that is:

$$\iint_S \mu(r,s)dr\,ds = \mathcal{E}(r,s) - \iint_{S^*} \mu(r,s)dr\,ds. \tag{14}$$

By exploiting the wiping out property, all the vertex of the staircase such that the constraint

$$\Delta y \geq \mathcal{E}_k(r,s) - \iint_{S^*} \mu(r,s)dr\,ds. \tag{15}$$

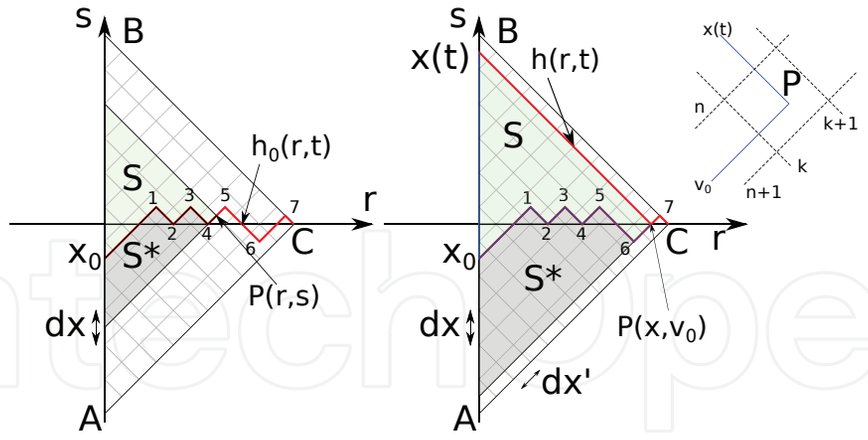

(a) State updating algorithm (b) Input computation by interpolation over the grid points

Figure 11. The algorithm of inversion of the Preisach operator

is fulfilled, are cancelled. The suffix k of he Everett function evidence the vertex of the triangle. In the case reported in Fig.11-(a) the initial state h_0 represented by the sequence of dominant extrema $\{0,1,2,3,4,5,6,7\}$ is updated and the vertex $\{0,1,2,3,4\}$ cancelled. So the state updating algorithm consists in applying the above condition and cancel all the vertex until it is verified. Once the last vertex has been cancelled, the following condition hold:

$$\Delta y = \mathcal{E}(x, v_0) - \iint_{S^*} \mu(r,s) dr\, ds. \tag{16}$$

being x the unknown value of the input field to be determined. In Fig. 11-(b) it is shown how $x(t)$ wipes out the vertex of the state function, and the operator attains the new state $h(r,t) = \{x, P, 7, C\}$ evidenced in red in the same figure where it is also shown a zoom of the new state around the point $P(x, v_0)$ lying within a square determined by the points $(n+1,k)$, $(n+1,k+1)$, (n,k) and $(n,k+1)$. As a first step, the Everett integrals at the points $(k+1,v_0)$ and (k,v_0) are found by linear interpolation:

$$\mathcal{E}(m, v_0) = \mathcal{E}(m,n) - (\mathcal{E}(m,n) - \mathcal{E}(m,n+1)) \frac{v_0 - n\Delta x'}{\Delta x'} \tag{17}$$

being $m = k+1$ and $m = k$. Finally, once these values have been determined, and exploiting eqn.(16) the final output value can be written as:

$$x' = \frac{\Delta y + \iint_S \mu(r,s) dr\, ds - \mathcal{E}(k, v_0)}{\mathcal{E}(k+1, v_0) - \mathcal{E}(k, v_0)} \Delta x' + k\Delta x', \tag{18}$$

where $x' = x/\sqrt{(2)}$ and $\Delta x' = \Delta x/\sqrt{(2)}$. For this reason the equation does not change when the variables without index are concerned. Moreover, it should be stressed that the integral in the previous equation is a known quantity. Such an approach requires only three linear interpolations at most and does not need any lengthy iteration. The procedure only requires the knowledge of the matrix storing the samples of the Everett integrals and its precision is linked to the mesh adopted for the Preisach plane or, in other words, to the number of measured samples used for the identification. Moreover, the algorithm, as already mentioned,

does not increase the computational weight of the algorithm which is equivalent to that of the direct operator.

4. Multi-variate systems with hysteresis

Smart materials, in general application conditions, cannot be considered as SISO systems, since each output quantity is a function of at least two input functions. For sake of example, in a magnetostrictive material the strain depends both on the mechanical load (stress) and magnetic field. A similar behavior can be experienced for the magnetic *flux density*. The behavior is illustrated in Fig. 12-(a) where the strain is affected by both the stress and field variation. Moreover, not only the H-field affects the internal state of the system, which is also altered by the applied stress, as shown by the hysteresis branches sketched in Fig. 12-(b). The experimental evidence witnessed by Figs. 2 and 12, allows to conclude

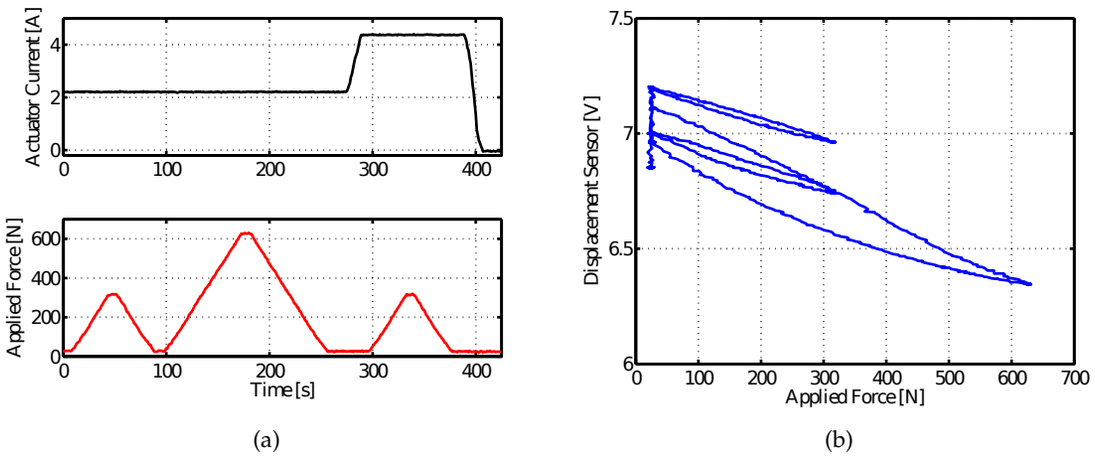

Figure 12. Applied current and force vs. time to a magnetostrictive sample (a); displacement/force hysteresis branches (b).

that the modeling of these systems requires a generalization of all the classical approaches to hysteresis phenomena. This need started two decades ago [1], [46] and yielded to models able to couple together two different input variables (i.e. ε and σ). This effort become of fundamental importance whenever the coexistence of non stationary stress and fields cannot be overlooked.

The simplest way to define more general models is to keep the usual SISO structure of systems with hysteresis, as the ones discussed in the previous section. To this aim, let us consider the mapping:

$$\zeta : (u, v) \in \mathcal{C}^0[0, T] \times \mathcal{C}^0[0, T] \rightarrow x \in \mathcal{C}^0[0, T], \tag{19}$$

where ζ is the operator relating the couple of continous functions (u, v), affecting the system behavior, to the input, x, of the memory operator, Θ. For the sake of example, in the case of a magnetostrictive material, ζ "links" the stress σ and magnetic field H to the input of the memory operator. Therefore

$$\mathcal{W} = \digamma \circ \Theta \circ \zeta, \tag{20}$$

represents a hysteresis operator with two inputs which generalizes the definition in [5] to a wider class of hysteresis operators. Before proceeding in the description of multi-variate systems with hysteresis in control applications, it is mandatory to provide some information

concerning its identification. To this aim, let us now consider the following operator, specified for a magneto-elastic material

$$y = F \circ \Theta \circ \zeta(x_1, x_2) + q(x_2), \tag{21}$$

where $y = \varepsilon$, $x_1 = H$, and $x_2 = \sigma$, being ε, H, and σ the strain, magnetic field and stress experienced by the material, respectively. Moreover, $q(\sigma)$ is a pure elastic response to be identified with almost trivial mechanical measurements at zero magnetic field. Even it is not strictly necessary, the latter assumption allows to take into account separately the effects of vertical translation of the magnetostrictive response due to pure mechanical reasons. Let us preliminary assume that the set of $j = 1, .., M$ anhysteretic[2] curves, e_j shown in Fig. 13-(b) is available. Moreover, assume that the interval of input variation ($x_2 = \sigma$) is $[\sigma_{min}, \sigma_{max}]$ and that the magnetostrictive response experiences a monotonic decrease for increasing compressive stresses, that is $\sigma_{min} = \sigma^*$. With reference to the figure, this corresponds to a 1.05 MPa applied mechanical stress. Finally, each curve is discretized into N samples such that $H_{i+1} - H_i = \Delta H$, with $i = 1, ..N$. Assuming further that $\zeta(H, \sigma^*) = H$ and $\lambda(\sigma^*) = 0$, if

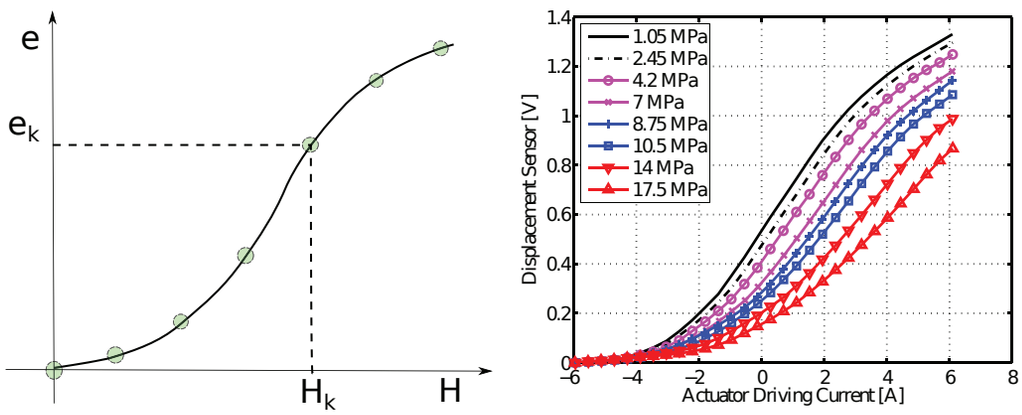

Figure 13. Example of *Anhysteretic* curve (a) Experimental Anisteretic curves for a magnetostrictive material (b).

$\sigma = \sigma^*$, then the operator takes the following classical form

$$e(t) \equiv \varepsilon(t) - q(\sigma) = F \circ \Theta[H], \tag{22}$$

which could be easily identified, according to the procedure sketched in sect. 2 and detailed in [28]. Once the Preisach distribution function is known, the procedure to identify the $\zeta(\cdot, \cdot)$ function can start. Recalling now that in suitable conditions $F \circ \Theta$ admits an inverse and that an efficient inversion algorithm is available, as shown in section 3, the eq. (22) can easily be re-arranged as:

$$\Gamma^{-1}[\varepsilon - q(\sigma)] = f(H, \sigma). \tag{23}$$

By this procedure, a set of $M \times N$ measured samples is now available, which enable us finding the samples $\zeta(H_i, \sigma_k)$ of the unknown function.

[2] It is defined as *anhysteretic*, the curve in the input-output plane, as in Fig. 13-(a), each point of which corresponds to the output of the $\mathcal{P}_0$ operator in the state represented by the horizontal curve $s = H_k$, that can be constructed by applying to the system the input $x(t)$ slowly converging to H_k

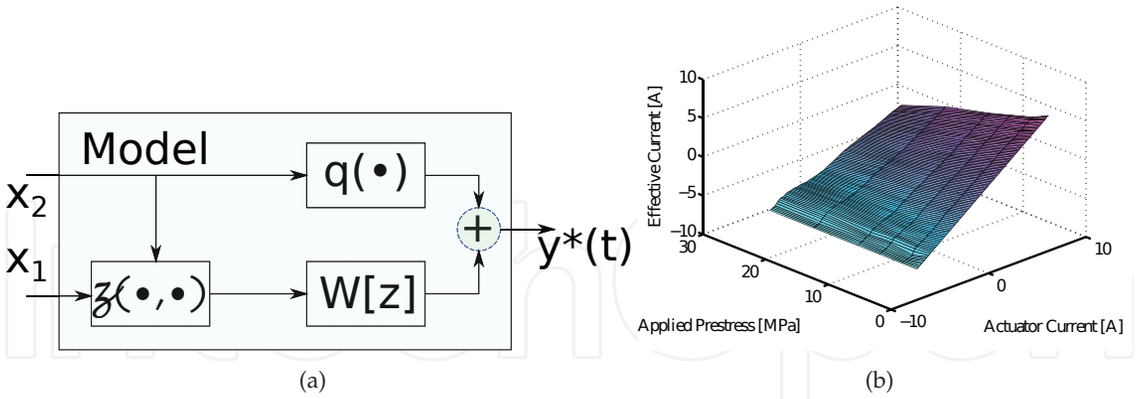

Figure 14. Block scheme of the 2-variables operator (a); Example of reconstruction of the ζ function, named as "effective current" in the vertical axis of the plot (b).

In order to show the effectiveness of the described procedure, it is important now to show the performances of a multi-variable model as the one described in eqn. (23). In particular, in Fig. 14-(b) it is shown the reconstructed ζ function, while in Fig. 14-(a), the scheme of the model is shown. It undergoes the input variable x_1 and x_2, according to eqn. (23), which in the specific case are the magnetic field and the stress, respectively. The output $y^*(t)$ is compared to the actual measured strain function and the results are sketched in Fig. 15. In particular, in Fig. 15-(a) it is shown the time variation of the input variables, i.e. $x_1(t) = H(t)$ and $x_2(t) = \sigma(t)$, in the first two frames, while in the third, it is described the output of the ζ-function, to which the hysteresis operator $\mathcal{W}$ is subject. In Fig. 15-(b) it is shown the system response, compared to the time behavior of the measured strain. Here the performances of the model described so far are compared to those of a model proposed in [10], where the dependence of memory on the stress is not taken into account.

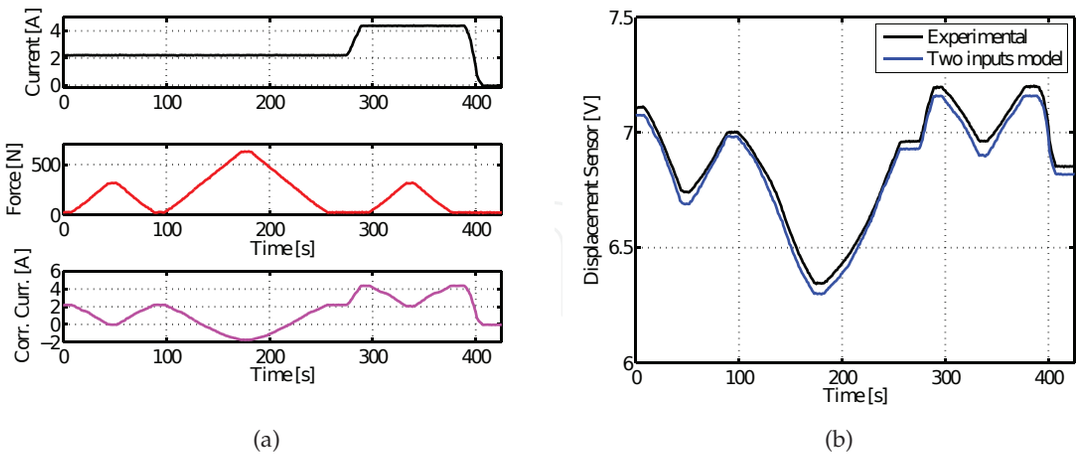

Figure 15. Comparison of the model's behavior to experiments for a prescribed history. Stress (load), magnetic field (curr) and ζ (corr-curr) vs. time (a); output displacement compared to the experimental data (b).

In conclusion of this section, it is worth to be further stressed that the procedure described so far is of general breath and can be exploited in modeling and compensation of any material/system with multi-variable hysteresis as most of multifunctional materials behave.

5. Model-based control strategies for smart actuators

After a complete review on the modeling and compensation strategies of actual systems with hysteresis, in general working conditions, has been settled, it is possible to discuss different approaches to their control through the definition of specific application frameworks. As a first step, let us start from the classical *model based* control approach, already sketched in Fig. 8, sect. 3

There, the employment of the compensation algorithm allows a easy design of the controller, which could be, as a first attempt, a classical PI system, with all its limits, but with the great advantage of its implementation neatness. This viewpoint has been widely used in smart actuation tasks where Piezo, SMAs or magnetostrictives were employed, [23, 24, 27, 35, 39]. In Fig. 16-(a) the whole control system is shown. In this figure, the block $D(s) = H(s)G(s)$ merge together the linear dynamic part of the actuator and the linear dynamic plant. So the series connection of $\mathcal{W}$ and $D(s)$ represents the *smart actuator* and the plant (SmA). This is a quite general scheme allowing to discuss the control system of the actuator both when loaded by the plant or *unloaded*. The part (b) of the same Fig. 16 shows the same system actuator-plant when it is affected by two inputs (x_1, x_2). The detailed discussion of this scheme will be provided later, at the end of this section.

In the example shown in Fig. 17 a triangular waveform with period $T = 0.02$ s is tracked by the control system sketched in Fig. 16-(a), with and without the compensation algorithm described in the previous sections, [12]. The effects of compensation evidence the increase of the tracking performances of the actuator. In [9] it is also discussed the improvements of the control performances also in term of stability.

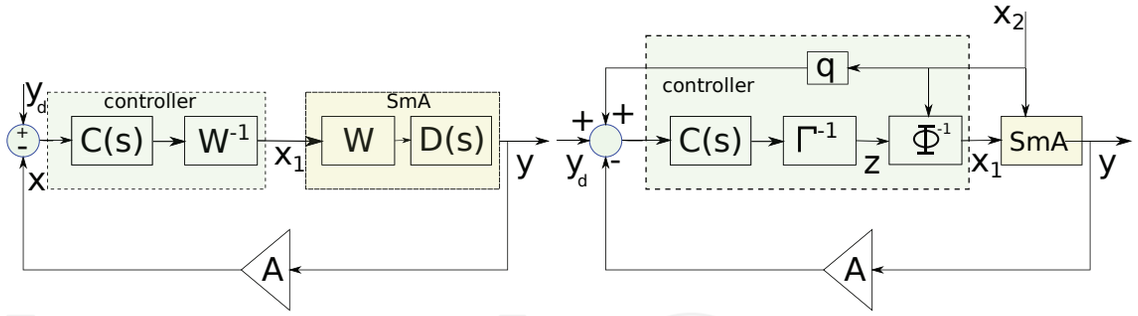

(a) Model-based control scheme (b) Control scheme with two variables feeding the Sma

Figure 16. Model-based control scheme (a) and its generalization to a multi-variable, model-based controller (b). In both cases, the smart actuator and the plant (SmA) are represented by the connection of $\mathcal{W}$ and $D(s)$

The examples considered until now refers to *slow* actuation applications, such as micro positioning tasks (cfr. also [8]). When the assumption of low input variation cannot be assumed as the general working condition, a more accurate discussion should be provided. To this aim, let us again consider the Fig 2, showing how the mechanical response of the material is strongly affected by the applied constant stress (i.e. the *pre-stress*). Normally the magnetostrictive material is subject to a prescribed (and optimal) stress, with the aim to maximize such response. When the actuator is working to actuate a prescribed mechanical load, the total stress experienced by the material has very low fluctuations with respect to the applied stress, whenever slow variations of the applied field are concerned. For high frequencies application tasks this assumption no longer holds and the material experiences

a simultaneous variation of stress and field. In that case the employment of a compensation algorithm with two variable is necessary. To this aim the *multi-variable* hysteresis modeling described in the section above could be an interesting starting point to define suitable multi-variable compensation and control strategies. A first attempt to tackle such a quite demanding problem was settled in [10], where a simple generalization of the Preisach model, taking into account the presence of a second variable (i.e. the stress) in the distribution function was stated and discussed. Such approach had the drawback that only a correction of the operator's output was concerned while no effects on the state were considered. It should be said, however, that even so the system showed promising characteristics, which yielded to further improvements and to the definition of the model described above (eqn. (21)). In the following we will sketch how the latter model can be employed to define suitable and well behaved multi-variable control strategies, [15–17]. However, a preliminary discussion to settle the existence conditions of the compensator for such a kind of multi-variable hysteresis operator is required. Let us now refer to the model specified in eqn. (21) which is re-arranged

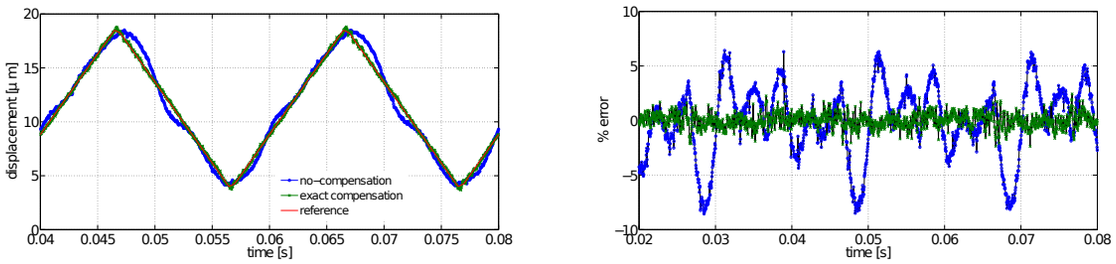

(a) Model-based control scheme

(b) Green: compensated control; Blue: uncompensated control

Figure 17. Model-based control scheme (a) and its performance in tracking a reference signal (b)

as follows:

$$z \equiv \mathcal{W}^{-1}[y-q] = \zeta(x_1, x_2), \tag{24}$$

where

$$\zeta : (x_1, x_2) \in \Omega \longrightarrow \mathbb{R}$$

is a continuous function and Ω the set where it is defined. Moreover, consider now the set where the above eqn. (24) admits at least one solution:

$$S = \left\{ (\bar{x}_2, \bar{z}) \in \mathbb{R}^2 : \exists x_1 \text{ with } \zeta(x_1, \bar{x}_2) \equiv \bar{z} \right\} \tag{25}$$

and the function:

$$\Phi : x_1 \in X \subseteq \mathbb{R} \longrightarrow (x_2, z) \in S. \tag{26}$$

It should be noticed that the latter defines a *single valued* function, being $\zeta(x_1, x_2)$ a *single valued* function. Moreover, recall that $e = y - q$ is the model's output without the pure mechanical response represented by $q(x_2)$.

This function could be either injective or not, depending on the characteristics of the real material, as evidenced hereafter. To this aim, let us consider the material, showing the relation between the output $y - q$ and the input variables x_1 and x_2 as shown in Fig. 18-(a). There with z it has been indicated the input variable corresponding to the output $y - q$ when $x_2 = x_2^*$. If now $x_2 = x_2'$ two distinct values of x_1 are obtained. This implies that the function Φ is *not injectve* (Fig 18-(b)). Conversely, if we refer to Fig. 19-(a), the value of x_1 corresponding

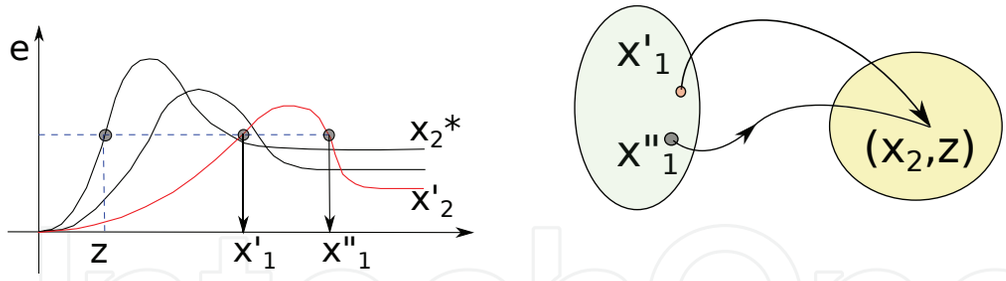

(a) Non monotone response characteristic of a general smart material.

(b) Example of non-injective Φ function

Figure 18. Example of the Φ function reconstructed from input-output available data. It can be stressed that the non-monotonicity of the response functions, as sketched in (a), yields to $\frac{\partial \zeta}{\partial x_1}$ that can assume any sign for assigned x_2

to a given z (which, as before, refers to the assigned value of output $y - q$ on the curve corresponding to $x_2 = x_2^*$), is now unique, when it exists. In fact in the same figure, the possibility that no x_1 values corresponding to a given couple (x_2, z) is also considered. This example evidences that not all values (x_2, z) belongs to the domain of definition of the function Φ. In this case the function is *injective* in S. Moreover, it would appear quite evident that the properties of the Φ function are strictly related to the monotonicity of the functions $(y - q) \leftrightarrow z$ or, in other words to the derivatives $\frac{\partial \zeta(x_1, x_2)}{\partial x_1}$, as detailed hereafter.

The function

$$z = \zeta(x_1, x_2)$$

can be rearranged by the aid of the function: $g : \mathbb{R}^2 \to \mathbb{R}^2$, having components:

$$\begin{cases} z = \zeta(x_1, x_2); \\ x = x_2, \end{cases} \tag{27}$$

and *Jacobian*:

$$J_g(x_1, x_2) = \begin{vmatrix} \frac{\partial \zeta}{\partial x_1} & \frac{\partial \zeta}{\partial x_2} \\ 0 & 1 \end{vmatrix} = \frac{\partial \zeta}{\partial x_1}. \tag{28}$$

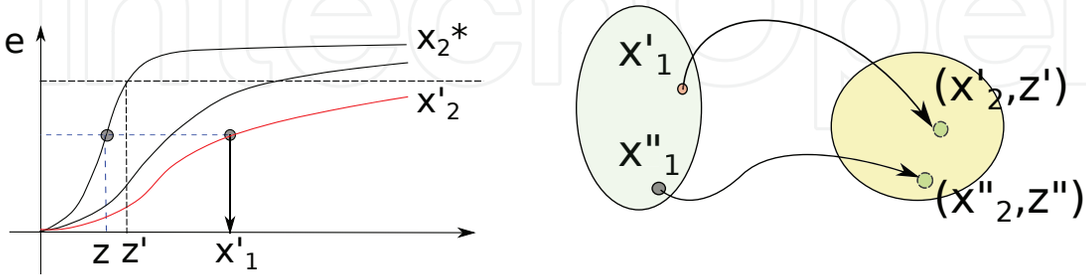

(a) Monotone response characteristic of a general smart material.

(b) Example of injective Φ function

Figure 19. Example of the Φ function reconstructed from input-output available data. It can be stressed that the strict monotonicity of the response functions, as sketched in (a), yields to $\frac{\partial \zeta}{\partial x_1} > 0$ for assigned x_2.

If now we define the set:

$$A = \{(P \equiv (x_1, x_2) \in \Omega : J(P) \neq 0\}, \tag{29}$$

it is possible to conclude that whenever A is a non-empty set, for every $P \in A$ the g function g is locally invertible and so the equation $\zeta(x_1, x_2) = z$ has only one x_1 solution. The sets

$$S^* = \left\{(\bar{x}_2, \bar{z}) \in \mathbb{R}^2 : (x_1, x_2) \in A\right\} \tag{30}$$

is a subset of S, i.e. $S^* \subseteq S$. As a consequence, Φ is injective in S^* and finally it admits the inverse function

$$\Phi^{-1} : S^* \longrightarrow X^*,$$

being X^* a subset of X. This line of reasoning shows the conditions which guarantee the existence of the Φ^{-1} function and hence the possibility to define the compensator of the 2-variables operator with hysteresis. This is a crucial point since only with this condition a generalization of the classical *model-based* control strategy can be settled for multi-variable systems with rate independent memory.

The availability of a procedure enabling the inversion of a hysteresis operator depending on two input variables opens the opportunity to extend *model-based* control strategies to systems having in realty two inputs (for example, desired strain and mechanical stress). This need arises in specific dynamic working conditions of magnetostrictives, (i.e. active vibration suppression of structures), where the device could experience forces of comparable magnitude of the applied stress, but could be extended to similar conditions involving different smart materials.

The simplest control strategy exploiting the results concerning the inversion of multi-variable hysteresis operators, is sketched in Fig. 16-(b). There we can observe the compensation algorithm described so far. In particular the operator Γ^{-1} which, in open loop, takes the variable $e = y - q$ and provides the corresponding input function for the reference case (i.e. $x_2 = x_2^*$), that is $x_1 = z$. The inverse of the Φ function, takes z and x_2 and provides the control variable x_1. If a given desired signal is provided, in presence of a time varying $x_2 = \sigma(t)$, the global behavior of the actuators drastically changes and, without a suitable *stress-dependent* compensation algorithm, the controller performances suddenly worsen. For the sake of example, in Fig. 20 it is shown the relative error in tracking a $\sin(t)/t$ function provided a time variation of the applied force over the full simulation time interval of about 400N. It is evident the improved behavior of the 2-variables control (2VC) system with respect to the case when stress corrections are not provided, [18]. The present approach allows to compensate the effects of nonlinearity and hysteresis in more general working conditions, guaranteeing a close-to-linear behavior of the actuator and making so easier the controller design. Unfortunately, the effects of the compensation algorithm together with the PI controller are beneficial for the whole control system whenever the desired signal is slowly varying, but its performances decrease for faster actuation purposes. Further, multi-variable compensation and control is mostly required exactly when faster signal to track are involved. Thus, different control schemes able to guarantee sufficient performances in a wider frequency range are necessary, [19, 22]. As a first attempt to address the issue, let us recall that closed loop control represents a necessary solution, in presence of disturbances model uncertainties, guaranteeing performances otherwise unachievable by open loop solutions. On the contrary, feedforward controls are easier to implement, do not affect the stability of the overall system

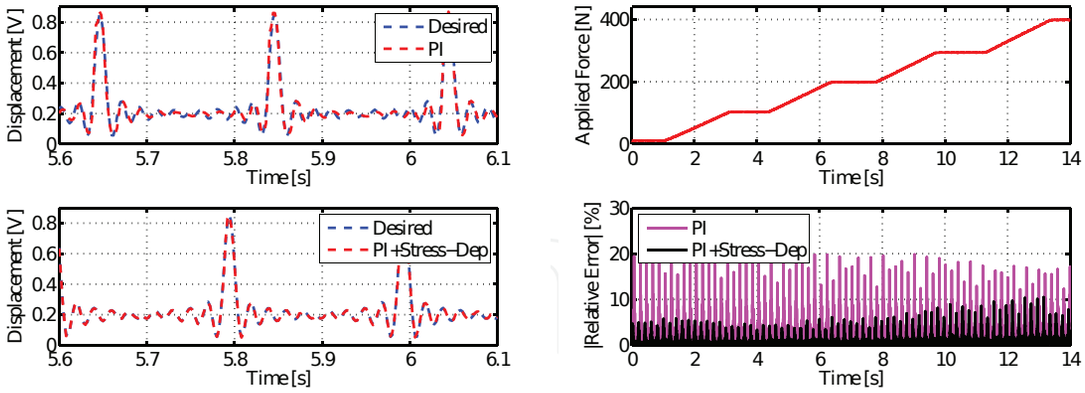

(a) Desired and measured output vs. time. Up: PI controller; bottom; PI+2VC (b) Applied stress and relative tracking error vs. time

Figure 20. Example of real time control task, by considering the effects of compensation with one or two variables

and show faster behavior with respect to feedback solutions since its action depends only on the feedforward controller and not on process dynamics. Modern control systems often employ both actions with the aim to obtain the advantages of both configuration, avoiding, as far as possible, their drawbacks so yielding to a controller with higher performances. Such a configuration is called *two-degrees-of-freedom*, 2-DoF, control system since in this way it is possible to design a controller that weights independently the reference signal and the measurements coming from the process [36, 38]. Examples of 2-DoF control systems for

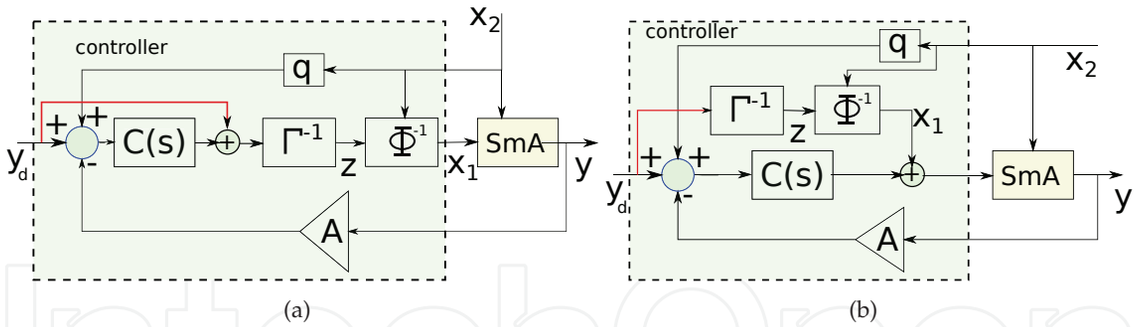

Figure 21. Block schemes of 2-DoF control systems. Hysteresis compensation on the feedback loop (a); Hysteresis compensation on the feedforward action (b)

actuators with memory, proposed in [19], are shown in Fig. 21. In both of the diagrams it is possible to locate a feedback and a feedforward action. In part -(a) of the figure, the feedforward action trivially consists in adding the desired output to the output of the linear controller $C(s)$. The compensation, is located on the feedback action. In that case both the compensator and actuator with hysteresis experiences exactly the same input history and so they share the same internal state. Conversely, the scheme reported on the part -(b) of the same figure shows the compensation located on the feedforward action, while the feedback loop is without compensation. In such a scheme it is quite evident that the real actuator and its compensator doesn't experiences the same input history. For this reason we could expect a different behavior with respect to the previous system.

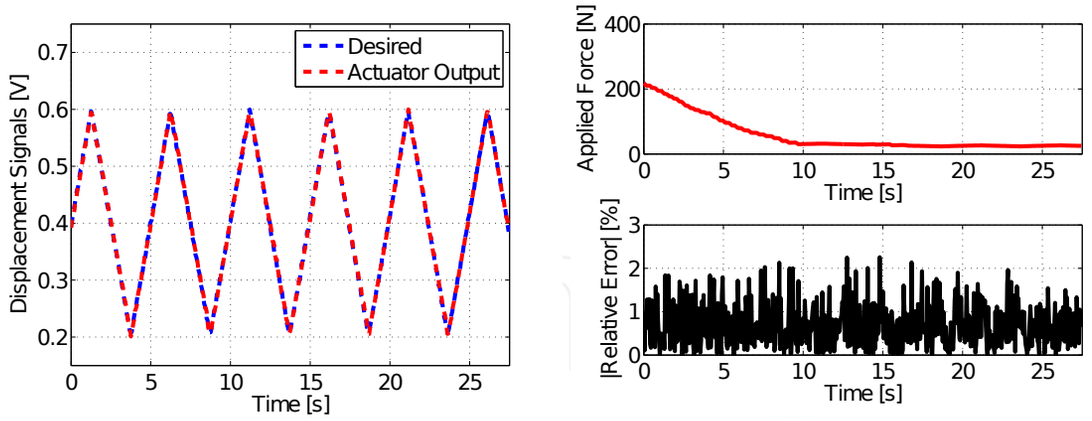

(a) (b)

Figure 22. Tracking performances of a PI control system with 2VC for low frequency application. In this case the period of the desired output is $T = 5$s

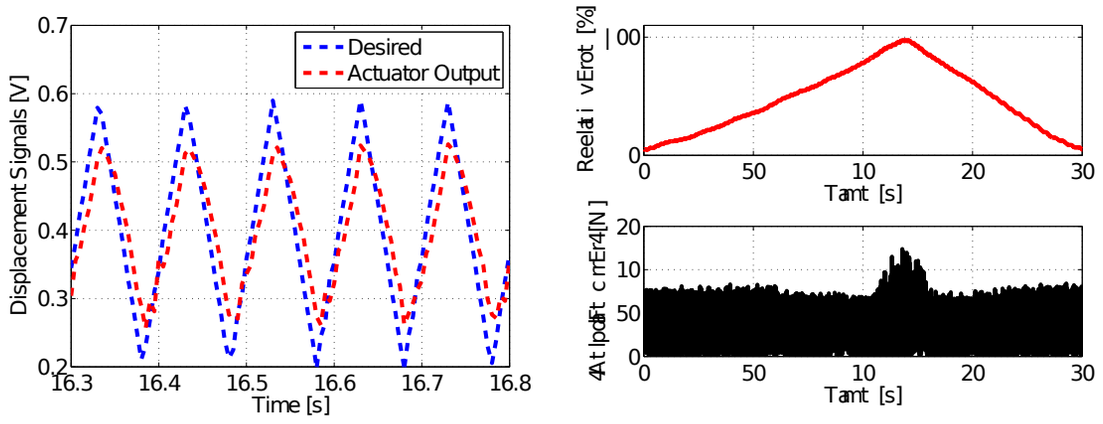

(a) (b)

Figure 23. Tracking performances of a PI control system with 2VC for higher frequency application. In this case the period of the desired output is $T = 0.1$s

In order to evidence the drawbacks of a classical feedback loop employing a simple PI controller, and the improvements provided by the 2-DoF control system, let us discuss the experiments performed by a *real-time* environment where the compensation algorithm and the PI controller are implemented in a PC with Matlab, and a xPC Target toolbox with a 16 bit acquisition/generation card are also employed. Further details are discussed in [19]. In particular, in Fig. 22 it is shown the performances of the feedback system, sketched in Fig. 16, in tracking a triangular waveform, with period of 5 s. Here the relative error lies below 3%. When the frequency is increased to 10Hz, the problems in tracking the same waveform dramatically arise and tracking error goes well beyond 15%, as evidenced in Fig 23. The performances results of the scheme reported in Fig. 21-(b) are shown in Fig. 24, with an increase of tracking performances. In Fig. 25, conversely, the performances of the 2-DoF control system presented in Fig. 21-(a) are shown. It can be observed a further increase of the tracking performances of the system with quite low tracking error, since the system provides the same state evolution of both the actuator and compensator.

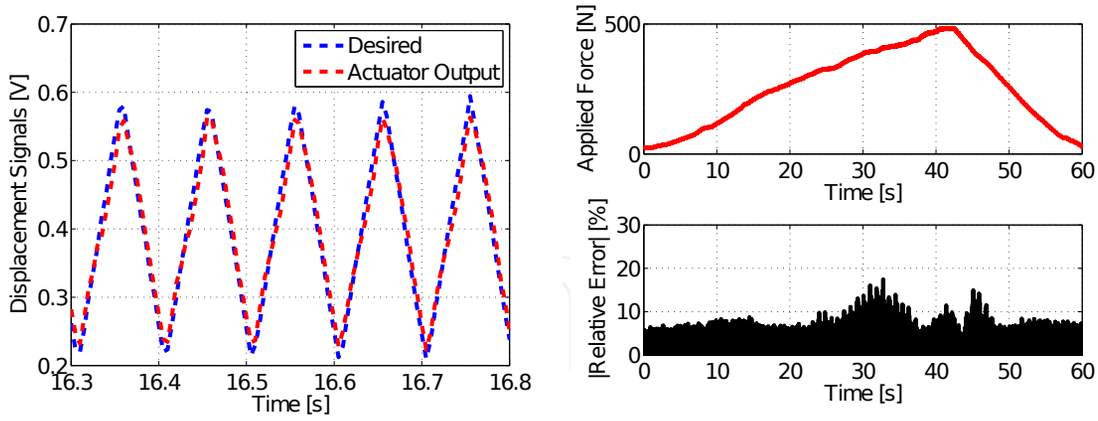

(a) (b)

Figure 24. Tracking performances of a 2-DoF control system with 2VC for higher frequency application. In this case the period of the desired output is $T = 0.1$s and the controller is specified in Fig. 21-(b)

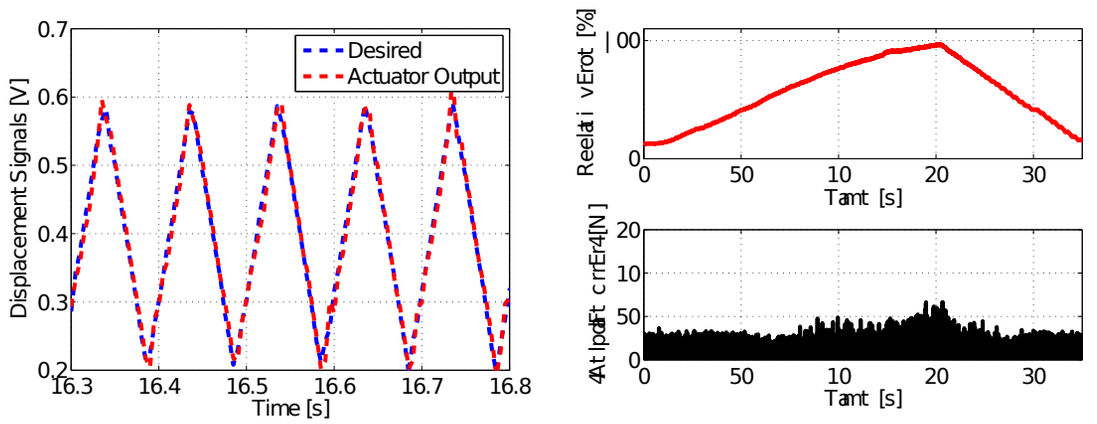

(a) (b)

Figure 25. Tracking performances of a 2-DoF control system with 2VC for higher frequency application. In this case the period of the desired output is $T = 0.1$s and the controller is specified in Fig. 21-(a)

In conclusion the availability of suitable and well assessed tools for the modeling and compensation of actuators with hysteresis enables to define control algorithms that fully exploits this high modeling capabilities. The result is the availability of a model-based control system which gather good performances and quite low computational effort, guaranteeing its suitability for real time and fast actuation tasks.

6. Conclusion

The chapter aimed to provide a view on the basic problems involved when modeling and control of smart materials, normally affected by memory phenomena, are concerned. So, after a brief review of some of the contributions provided in this field, the attention was focused specifically on materials showing a magnetostrictive behavior, such as Terfenol-D and Galfenol. However, all the ideas and tools introduced and discussed could be widely exploited for other smart materials with non-negligible memory effects.

In Sect. 2 a brief description of the phenomena involved in magnetostrictive materials is drawn and the ideas of their modeling are also provided. In this respect, the basic operators describing systems with hysteresis is presented, with a specific attention to the classical Preisach model. Although the most known and applied approach is the one in the 'rotated' system of coordinates, according to Mayergoyz's book, [28], the adopted formalism allover the chapter is that preferred in the books [7] and [26], showing some interesting characteristic from the modeling viewpoint. In any case, the relationship between them is explicitly pointed out.

In the next section 3 the attention is focused on the main modeling and compensation issues which are normally adopted for control purposes. Here, a specific attention is devoted to the congruency property of Preisach operator, which forces a specific attention in the inversion of the operator. Finally, a basic point is discussed with some detail, that is, the definition of compensation algorithms which doesn't require further computational effort with respect to the 'direct' operator, i.e. the Preisach operator. This specific point becomes crucial when a *model-based* real time control approach is of concern.

In order to put the issues discussed in the chapter in the current framework of smart materials and devices, in section 5 the need to manage two independent variables in controlling the device is emphasized, by proposing a well-behaved procedure to handle the stress and magnetic field simultaneously. The effectiveness of this approach for a more precise description and control of smart devices is also discussed by comparison to measured data. Such discussion paves the way to the last section of the chapter, where some application in *real time* controlling smart materials are presented. In particular, 'standard' and 2-DoF control strategies are presented, all fulfilling the constraint to keep a low computational complexity of the whole control system, still ensuring good tracking and stability performances.

Author details

Daniele Davino, Alessandro Giustiniani, Ciro Visone
University of Sannio - Engineering Department, 82100 Benevento (BN), Italy

7. References

[1] Adly, A.A., Mayergoyz, I.D. & Bergqvist, A. (1991). Preisach modeling of magnetostrictive hysteresis *AIP Journal of Applied Physics* 69, 5777.
[2] Anton, S.R. & Sodano, H.A. (2007). A review of power harvesting using piezoelectric materials (2003-2006), *IOP Smart Materials and Structures*, vol. 16, 3, pp. R1-R21.
[3] Bar-Cohen, Y. (2002). Electro-active polymers: Current capabilities and challenges, *Proceedings of SPIE*, San Diego, CA.
[4] Bellouard, Y. (2008). Shape memory alloys for microsystems: A review from a material research perspective *ELSEVIER Materials Science and Engineering A* 481-482, pp. 582-589.
[5] Bergqvist, A. & Engdahl, G. (1991). A stress-dependent magnetic Preisach hysteresis model, *IEEE Transactions on Magnetics*, Vol. 27, No. 6, pt 2, pp. 4796-4798.
[6] Brokate, M. (1989). Some mathematical properties of the Preisach model of hysteresis, *IEEE Transactions on Magnetics*, 25, pp. 2922-24.
[7] Brokate, M. & Sprekels, J. (1996) *Hysteresis and Phase Transitions*,Springer.
[8] Cavallo, A., Natale, C. Pirozzi, S. & Visone, C. (2003). Effects of Hysteresis Compensation in Feedback Control Systems, *IEEE Transactions on Magnetics* Vol. 39, No. 3, pp.1389-1392.

[9] Cavallo, A., Natale, C., Pirozzi, S., Visone, C. & Formisano, A. (2004). Feedback Control Systems for Micropositioning Tasks With Hysteresis Compensation, *IEEE Transactions on Magnetics*, Vol. 40, No. 2, pp. 876-879.
[10] Cavallo, A., Davino, D., De Maria, G., Natale, C., Pirozzi, S. & Visone, C. (2008). Hysteresis compensation of smart actuators under variable stress conditions, *ELSEVIER Physica B*, 403, 2-3, pp. 261-265.
[11] Chung, D.Y., Hogan, T., Brazis, P., Rocci-Lane, M., Kannewurf, C., Bastea, M., Uher, C. & Kanatzidis, M. G. (2000). $CsBi_4Te_6$: A High-Performance Thermoelectric Material for Low-Temperature Applications, *Science* 287, pp. 1024-27
[12] Davino, D., Natale, C., Pirozzi, S. & Visone, C. (2005). A fast compensation algorithm for real-time control of magnetostrictive actuators, *ELSEVIER Journal of Magnetism and Magnetic Materials*, 290-291, pp. 1351-54.
[13] Davino, D., Giustiniani, A. & Visone, C. (2008). Fast Inverse Preisach Models in Algorithms for Static and Quasistatic Magnetic-Field Computations, *IEEE Transactions on Magnetics*, 44 (6) , pp. 862-865.
[14] Davino, D., Giustiniani, A. & Visone, C. (2008). Properties of Hysteresis Models Relevant in Electromagnetic Fields Numerical Solvers, *ELSEVIER Physica B: Condensed Matter*, 403 , pp. 414-417.
[15] Davino, D., Giustiniani, A. & Visone, C. (2008). A Magnetostrictive Model with Stress Dependence for Real-Time Applications, *IEEE Transactions on Magnetics*, 44 (11-2) , pp. 3193-3196.
[16] Davino, D., Giustiniani, A. & Visone, C. (2009). Experimental Properties of an Efficient Stress-Dependent Magnetostriction Model, *AIP Journal of Applied Physics*, 105 (07D512) , pp. 1-3.
[17] Davino, D., Giustiniani, A. & Visone, C. (2010). Design and Test of a Stress Dependent Compensator for Magnetostrictive Actuators, *IEEE Transactions on Magnetics*, 46 (2) , pp. 646-649.
[18] Davino, D., Giustiniani, A. & Visone, C. (2011). Compensation and control of two-inputs systems with hysteresis, *IOP Journal of Physics: Conference Series*, 268, doi:10.1088/1742-6596/268/1/012005.
[19] Davino, D., Giustiniani, A., Iannelli, L. & Visone, C. (2012). Comparison of real-time control strategies with hysteresis compensation for magnetostrictive actuators, *IOS International Journal of Applied Electromagnetics and Mechanics*, in press.
[20] Dlala, E. & Arkkio, A. (2006). Inverted and forward Preisach models for numerical analysis of electromagnetic field problems, *IEEE Transactions on Magnetics*, Vol. 42, No. 8, pp. 1963-1973.
[21] Engdhal, G. (editor) (2000) *Handbook of Giant Magnetostrictive Materials*, Academic Press.
[22] Esbrook, A., Guibord, M., Tan, X. & Khalil, H.K. (2010). Control of systems with hysteresis via servocompensation and its application to nanopositioning, *Proceedings of the 2010 American Control Conference, ACC 2010*, Article number 5531422, Pages 6531-6536.
[23] Ge, P. & Jouaneh, M. (1996). Tracking Control of a Piezoceramic Actuator, *IEEE Transactions On Control Systems Technology*, 4, pp. 209.
[24] Hasegawa, T. & Majima, S. (1998). A control system to compensate the hysteresis by Preisach model on SMA actuator, *Proceedings of IEEE International Symposium on Micromechatronics and Human Science*, 171.
[25] Krasnoselskii, M. A. & Pokrovskii, A. V. (1989). Systems with Hysteresis, Springer-Verlag.

[26] Krejci, P. (1996). Hysteresis, convexity and dissipation in hyperbolic equations, *Gakuto Int. Series Math. Sci. & Appl.*, 8, Gakkotosho, Tokyo.
[27] Krejci, P. & Kuhnen, K. (2001). Inverse control of systems with hysteresis and creeps, *Proceedings of Control Theory and Applications*, Vol. 148, No. 3, pp. 185-192.
[28] Mayergoyz, I. D. (1991) *Mathematical Models of Hysteresis*, Springer.
[29] Miano, G., Serpico, C. & Visone, C. (1997). A new model of magnetic hysteresis, based on Stop hysterons: an application to magnetic field discussion, *IEEE Transactions on Magnetics*, Vol. 32, No. 3, pp. 1132-1135.
[30] Natale, C., Velardi, F. & Visone, C. (2001). Identification and compensation of Preisach hysteresis models for magnetostrictive actuators, *ELSEVIER Physica B*, 306, pp. 161-165.
[31] Otsuka, K. & Wayman, C.M. (1998) *Shape Memory Materials*, Cambridge University Press.
[32] Panda, P. K. (2009). Review: environmental friendly lead-free piezoelectric materials, *SPRINGER Journals of Matererials Science*, 44, pp. 5049-5062, DOI 10.1007/s10853-009-3643-0.
[33] Pecharsky, V.K. & Gschneidner, K.A. (2006). Advanced magnetocaloric materials: What does the future hold? *International Journal of Refrigeration* 29 pp. 1239-1249.
[34] Polla, D.L. & Francis, L.F. (1998). Processing And Characterization Of Piezoelectric Materials And Integration Into Microelectromechanical Systems, *Annual Review Matererials Science*, 28, pp. 563-597.
[35] Schafer, J. & Janocha, H. (1995). Compensation Of Hysteresis In Solid-State Actuators, *ELSEVIER Sensors And Actuators A* 49, pp. 97-102.
[36] Skogestad, S. & Postlethwaite, I. (2005). Multivariable Feedback Control: Analysis and Design, *Wiley-Interscience*.
[37] Söderberg, O., Ge, Y., Sozinov, A., Hannula, S.P. & Lindroos, V.K. (2005). Recent breakthrough development of the magnetic shape memory effect in Ni-Mn-Ga alloys *IOP Smart Materials and Structures* 14, 5.
[38] Sugie, T. & Yoshikawa, T. (1986). General solution of robust tracking problem in two-degree-of-freedom control systems *IEEE Transactions on Automatic Control*, Vol. 31 (6), pp. 552-554.
[39] Tan, X., Venkataraman, R. & Krishnaprasad, P.S. (2001). Control of hysteresis: Theory and experimental results, SPIE Modeling, Signal Processing, and Control in Smart Structures (Rao V. S., Ed.), 4326, pp. 101-112.
[40] Tellinen, J., et al., (2002). Basic properties of magnetic shape memory actuators, *Proceedings of 8th ACTUATOR Conference*, Bremen, Germany.
[41] Visintin, A. (1991) *Differential Models of Hysteresis*, Springer.
[42] Visone, C. & Serpico, C. (2001). Hysteresis operators for the modeling of magnetostrictive materials, *ELSEVIER Physica B: Condensed Matter*, 306 (1-4) , pp. 78-83.
[43] Visone, C. & Sjostrom, M. (2004). Exact invertible hysteresis models based on play operators, 2004, *ELSEVIER Physica B: Condensed Matter*, 343, pp. 148Ð52.
[44] Visone, C. (2008). Hysteresis Modelling and Compensation for Smart Sensors and Actuators, *IOP Journal of Physics Conference Series*.
[45] Webb, G.V., Lagoudas, D.C. & Kurdila, J. (1998). Hysteresis modeling of SMA actuators for control applications, *SAGE Journal of Intelligent Material Systems and Structures*, Vol. 9, No. 6, pp. 432-48.
[46] Webb, G., Lagoudas, D. & Kurdila, A. (1999). Adaptive hysteresis compensation for SMA actuators with stress-induced variations in hysteresis, *SAGE Journal of Intelligent Material Systems and Structures*, Vol. 10, No. 11, pp. 845-854.